IEEE Access
Multidisciplinary | Rapid Review | Open Access Journal

Date of publication xxxx 00, 0000, date of current version xxxx 00, 0000.

Digital Object Identifier 10.1109/ACCESS.2021.DOI

Cooperative Load Transportation with Two Quadrotors Using Adaptive Control

DANIEL KHEDE DOURADO VILLA[1], ALEXANDRE SANTOS BRANDÃO[2], RICARDO CARELLI[3], (SENIOR MEMBER, IEEE), AND MÁRIO SARCINELLI-FILHO.[4]

[1]Graduate Program on Electrical Engineering, Federal University of Espírito Santo, Vitória, ES, 29.075-910, Brazil (e-mail: danielkdv@gmail.com)
[2]Department of Electrical Engineering, Federal University of Viçosa, Viçosa, MG, 36570-900, Brazil (e-mail: alexandre.brandao@ufv.br)
[3]Institute of Automatics, National University of San Juan, J5400ARL, Argentine (e-mail: rcarelli@inaut.unsj.edu.ar)
[4]Department of Electrical Engineering, Federal University of Espírito Santo, Vitória, ES, 29.075-910, Brazil (e-mail: mario.sarcinelli@ufes.br)

Corresponding author: Mário Sarcinelli-Filho (e-mail: mario.sarcinelli@ufes.br).

ABSTRACT The problem of carrying a bar-shaped payload suspended by flexible cables attached to two quadrotors is analyzed in this work. The aerial vehicles and the load are dealt with as a single system, whose kinematics is described as a multi-robot formation using the virtual structure approach. The dynamic effects caused by the tethered load over the quadrotors, as well as those caused by each quadrotor over the other, are treated by an adaptive dynamic compensator. To validate the proposal, experiments were run testing the system in adverse conditions: transportation far from quasi-static motion, high payload-to-quadrotor weight ratio, 20% of error in the robot model parameters, transportation under wind disturbances, and payload weight changes during flight. The good performance of the proposed control system in all these tests allows concluding that the proposed system is able to accomplish payload positioning, orientation, and trajectory tracking under adverse conditions, with accelerations up to 1.6 m/s^2.

INDEX TERMS Multi-agent systems, Payload, Cable-suspended, UAV-Formation control, Nonlinear control, Aerial robotics

I. INTRODUCTION

An emerging application of unmanned aerial vehicles (UAVs) is the use of quadrotors to grasp, manipulate, and transport payloads [1]–[4]. Commonly, this can be achieved using one out of two strategies: by tethering the payload to the vehicle body, characterizing a cable-suspended load transportation, or by attaching the load directly on the body of the vehicle, characterizing a grasped load transportation. In the first case, the number of underactuated degrees of freedom increases, but the agility of the vehicle to maneuver is preserved. As for the second case, it is easier to obtain the mathematical model of the system, but the inertia of the vehicle is increased, thus decreasing its agility to maneuver. There are successful works considering both strategies, using a single agent [5]–[7] or even a team of agents [8]–[10] carrying payloads. Specifically talking about a team of quadrotors carrying a payload, the focus of this work, the main advantages are the viability of carrying a load that is too heavy for the thrust capability of a single quadrotor, and the possibility of increasing redundancy and safety.

As discussed in the survey presented in [4], in spite of the feasibility, there are many open challenges regarding the transportation of slung loads by quadrotors. Carrying a cable-suspended payload demands that the controllers deal with a pendulum stabilization problem while flying. In addition, it is hard to obtain a generic mathematical model for this task,

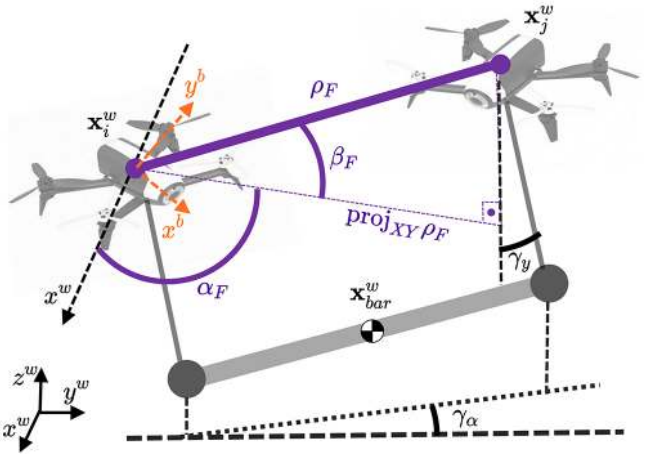

FIGURE 1. Virtual structure formation for two UAVs carrying a payload. The virtual structure is depicted in purple.

once it can be divided into three flight modes: (i) lifting, (ii) transportation, and (iii) delivery, which have distinct dynamic characteristics and are affected by the weight and shape of the load. Moreover, for a squad of agents, the controllers should be robust enough to keep tracking of a desired trajectory under load swings and to deal with the forces each agent exerts on the others.

A. RELATED WORK

Recent publications proposed control solutions for the manipulation and transportation of suspended payloads using quadrotors working cooperatively. In [11]–[13], for instance, the position and attitude of the payload are controlled in a cable-driven parallel robot fashion, whereas an approach without communication is presented in [14], [15], using force feedback to control the pose of the payload. In [16]–[20], by its turn, the manipulation task is performed by a quadrotor formation, which allows easy configuration and trajectory/task planning for the robots; while in [21] a force-based consensus algorithm ensures an equal share of the payload mass among the quadrotors in the formation. Despite their impressive contributions, to be able to handle the different transportation flight modes and perform trajectory tracking and path following at velocities suitable for real-world applications, the robustness of these techniques still needs to be improved.

Accordingly, a control algorithm that provides robustness in the presence of model uncertainties and external disturbances is certainly a reasonable option for load transportation. Different strategies have been used to achieve this for quadrotors carrying suspended payloads. As an example, in [22] reinforcement learning was used to achieve end-to-end (i.e., from load pick-up to delivery) payload transportation, where a meta-learning method updates the dynamic model of the system whenever variations of the payload occur. Reinforcement learning was also used in [23] to transport payloads by a team of three quadrotors, in which learning was used for planning smooth and swing-free trajectories. In [24]–[26], by their turn, adaptive control was used to counteracts the model parameter uncertainties by adjusting them in real-time, also allowing quick adaptation to new dynamics in pick-up or delivery tasks. Moreover, many authors achieved impressive results in terms of robustness using energy-based and passivity-based approaches for load transportation, as in [27]–[30], to cite a few, where damping is injected to dissipate undesired energy and achieve stability. Another common approach employed to obtain robustness is the use of sliding mode controllers. This technique turns the system not susceptible to uncertainties by driving its states to a switching surface in the state space. The authors of [31] and [26] demonstrated that for applications considering a single vehicle and cooperative transportation.

Nevertheless, these controllers have some drawbacks with respect to their practical application. Learning algorithms suffer to deliver generalized solutions, requiring exhaustive real-world training under diverse environmental conditions, whereas normally the training data are obtained indoor or running a system simulation using traditional dynamic models. Regarding adaptive controllers, as they adapt themselves online for optimal model parameters, a solid prior knowledge of the structure of the system model is essential. With regard to passivity-based approaches, despite their success on disturbance rejection for load stabilization, they still lack experimental validation at velocities/accelerations suitable for real-world applications, once they have been tested only in quasi-static motion. As for sliding mode controllers, although being quite robust they are inherently flawed to deliver smooth solutions due to the chattering effect, which may cause vibration and load oscillation.

B. CONTRIBUTIONS

In such a context, the main objective of this work is the proposal of a robust and simple control system for two quadrotors working cooperatively to carry a suspended rod-shaped payload, as depicted in Figure 1. The kinematics of the quadrotors are managed as a robot formation problem, and a virtual structure formation in combination with a kinematic controller handles the desired position and velocity for the vehicles, to which the load is attached through cables.

Among the robust controller drawbacks discussed in Subsection I-A, those associated with adaptive controllers seem to us to be the more amendable from a practical viewpoint, once the model structure for a variety of tasks using quadrotors is a well-discussed subject in the literature (such as the dynamic models found in the references of this paper). Thus, to improve the tracking of the velocity references given by the kinematic controller responsible to guide the formation, an adaptive dynamic compensator is proposed for each UAV in the formation to deal with the model uncertainties.

The main contributions of this paper can be summarized as follows: (i) we provide a simple method for planning the transportation missions, allowing the operator to directly plan for navigation of the payload center-of-mass and payload orientation using the virtual structure formation paradigm (see Figure 2); in addition, the virtual structure formation is easily interchangeable for different loads being carried and cable lengths; (ii) the adaptation law is updated online, thus allowing real-time compensation for thrust-related uncertainties and drag-related disturbances; (iii) our controller requires no sensory data related to the payload; and (iv) we provide a comparative survey relating the main features found in the recent works regarding load transportation with quadrotors, which also highlights two experimental contributions of this work: transportation far from quasi-static motion, tracking 3D desired trajectories in accelerations up to 1.6 m/s^2, and transportation with payload-to-quadrotor weight ratio up to 0.575, far from the weight ratio usually found in other works of the literature.

To discuss such topics the paper is hereinafter split in a few sections, starting with Section II, which characterizes the formation adopted. Following, Section III describes the kinematic controller in charge of dealing with how the forma-

This article has been accepted for publication in a future issue of this journal, but has not been fully edited. Content may change prior to final publication. Citation information: DOI 10.1109/ACCESS.2021.3113466, IEEE Access

tion as a whole should behave, whereas Section IV discusses the system dynamics and Section V presents the adaptive dynamic compensation module associated to each quadrotor in the formation. In the sequel, Section VI discusses the setup adopted for running the validating experiments, whereas Section VII shows and discusses the results of the experiments run. Finally, Section VIII highlights the main conclusions of the work.

II. MULTIPLE ROBOT FORMATION

As our system considers two UAVs cooperatively carrying a bar-shaped payload, we choose to formulate this problem as a robot formation problem, rather than individually plan desired trajectories that synchronizes the robots for the task. Therefore, we just need to obtain the formation navigation references from the task planner whereas the references for the robots are generated by a formation kinematic controller, whose stability is demonstrated. The proposed formation framework is based on the virtual structure paradigm [32], for which the virtual structure is a line in the 3D space, the line linking the two UAVs. Such a line is characterized by the so-called formation variables, which are here referred to as

$$\mathbf{q} = [\mathbf{q}_p^\top \quad \mathbf{q}_c^\top]^\top \in \mathbb{R}^6, \tag{1}$$

where $\mathbf{q}_p = [x_F \; y_F \; z_F]^\top \in \mathbb{R}^3$ represents the position coordinates of the virtual structure in the world frame, here given by the position of one of the UAVs in the formation extremities, whereas $\mathbf{q}_c = [\alpha_F \; \beta_F \; \rho_F]^\top \in \mathbb{R}^3$ are the formation configuration that defines the other extremity, as it can be seen in Figure 1. As for the formation configuration components, α_F is the angle between the X-axis and the projection of the virtual structure on the XY-plane, β_F is the angle between the XY-plane and the virtual structure, and ρ_F is the length of the virtual structure (the distance between the two UAVs).

In summary, the position of a UAV with respect to the other is given by a set of spherical variables, and the payload is considered hanging below the virtual structure formation at a distance $-\ell\hat{\mathbf{z}}^w$, defined by the length of the cables. Considering that the system is in internal equilibrium, the payload orientations in yaw and pitch are given by α_F and β_F. Also, the positions of the two attachment points in the payload coincide with the horizontal positions of the vehicles, and, if a homogeneous payload is symmetrically attached by the cables, its center-of-mass (CoM) is collinear with the centroid of the virtual structure, which is given by

$$\mathbf{x}_{bar} = \mathbf{q}_p + \mathbf{x}_{bar/q}\,, \text{ with } \mathbf{x}_{bar/q} = \begin{bmatrix} \frac{1}{2}\rho_F c_{\alpha_F} c_{\beta_F} \\ \frac{1}{2}\rho_F s_{\alpha_F} c_{\beta_F} \\ \frac{1}{2}\rho_F s_{\beta_F} - \ell \end{bmatrix}, \tag{2}$$

where $s_{\alpha_F} = \sin\alpha_F$ and $c_{\alpha_F} = \cos\alpha_F$, with $\mathbf{x}_{bar/q}$ being the vector that maps the formation position coordinates into the payload center-of-mass.

Defining the desired state for the formation as $\mathbf{q}_{des} = [\mathbf{q}_{p,des}^\top \; \mathbf{q}_{c,des}^\top]^\top \in \mathbb{R}^6$, and the commanded reference state as $\dot{\mathbf{q}}_{ref} \in \mathbb{R}^6$, two task-planning approaches can be used to deal with the transportation task here addressed. One of them consists in dealing with the formation states directly, what means to deal with $\mathbf{q}_{des}$, knowing that, after stabilization, the payload will be hanging below the formation, whereas the other consists in controlling a point in the payload (its center-of-mass, for instance), from which the desired formation states can be obtained in a way similar to the one that generated (2). This setup allows the UAV formation and payload to be used for complex transportation, capable of tracking desired trajectories and paths, and allowing transportation in limited spaces, where it is necessary to tilt and turn the load to avoid collisions. Some examples for the system configuration $\mathbf{q}_c$ are provided in Figure 2.

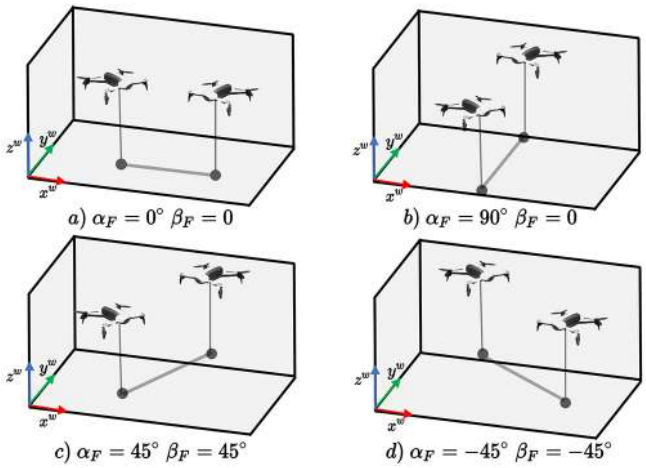

FIGURE 2. Virtual structure formation at different configurations for two UAVs carrying a payload.

To control the formation and vehicles, an inner-outer loop control scheme is adopted, which is illustrated in Figure 3. The outer loop corresponds to a kinematic controller, which generates the formation reference velocities $\dot{\mathbf{q}}_{ref}$, based on the desired formation position and configuration and their time derivatives. In the sequel, an inverse Jacobian matrix maps these formation reference signals into velocity references for the two vehicles. Then, the references thus obtained for the vehicles are treated by an adaptive dynamic compensation module, responsible for considering the dynamics of the vehicles and counteracting the dynamic effects caused by the payload and by one vehicle on the other.

III. FORMATION KINEMATIC CONTROL

Defining the error between the desired formation state and the current formation state as $\tilde{\mathbf{q}} = \mathbf{q}_{des} - \mathbf{q}$, the control law

$$\dot{\mathbf{q}}_{ref} = \dot{\mathbf{q}}_{des} + \kappa_1 \tanh(\kappa_2 \tilde{\mathbf{q}}) \tag{3}$$

is proposed for the kinematic formation controller, where κ_1 and κ_2 are positive definite diagonal matrices, and $\tanh(\cdot)$ is used as a smooth saturation function. During robot navigation, a feedback loop updates the formation entries at each control cycle, thus changing the current state of the formation. To compute the formation control feedback, the relationship between the robots space and formation space

This article has been accepted for publication in a future issue of this journal, but has not been fully edited. Content may change prior to final publication. Citation information: DOI 10.1109/ACCESS.2021.3113466, IEEE Access

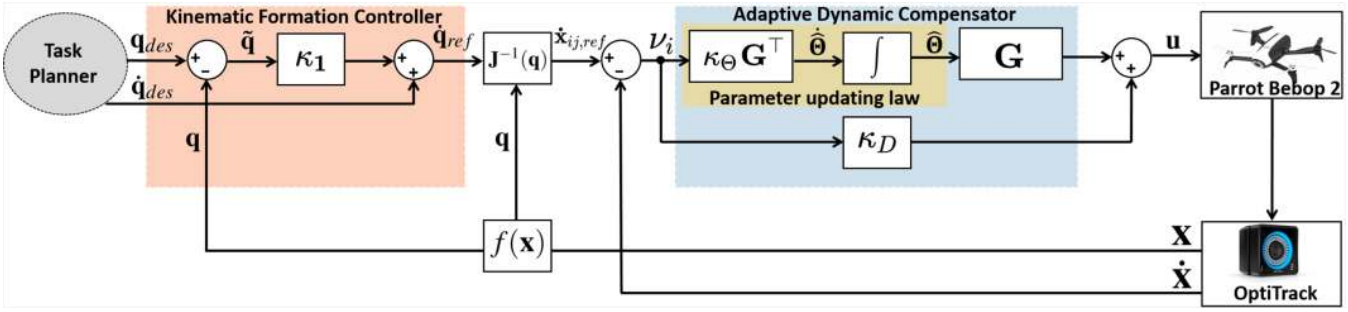

FIGURE 3. Inner-outer loop control system for the virtual structure formation and the quadrotors. The outer loop kinematic controller generates the velocity reference $\dot{\mathbf{q}}_{ref} \in \mathbb{R}^6$ using the payload desired pose and velocity (defined by the user). Thus, a Jacobian matrix maps these references into velocity references for the vehicles, $\dot{\mathbf{x}}_{ref} \in \mathbb{R}^6$, where the first three elements are inputs for the quadrotor 1, and the last three for the quadrotor 2. Finally, these velocity references become acceleration references for a dynamic compensator, using the control scheme presented in Section V-A.

should be known. Such a relationship is characterized by $\mathbf{q} = f(\mathbf{x}_{ij})$, with

$$\mathbf{q} = f(\mathbf{x}_{ij}) = \begin{bmatrix} x_i \\ y_i \\ z_i \\ \text{atan2}\left(\frac{y_j - y_i}{x_j - x_i}\right) \\ \text{atan2}\left(\frac{z_j - z_i}{\sqrt{(x_j - x_i)^2 + (y_j - y_i)^2}}\right) \\ ||\mathbf{x}_j - \mathbf{x}_i||_2 \end{bmatrix}, \tag{4}$$

where $\mathbf{q}$ is a vector containing the formation variables (characterizing the the formation space) and $\mathbf{x}_{ij} = [\mathbf{x}_i^\top \ \mathbf{x}_j^\top]^\top \in \mathbb{R}^6$ is a vector containing the positions of the robots (characterizing the robots space), with i, j representing the quadrotors, and with $\mathbf{x}_i = [x_i \ y_i \ z_i]^\top \in \mathbb{R}^3$ representing the position coordinates of the i-th quadrotor in the world frame.

To map the formation references, $\dot{\mathbf{q}}_{ref}$, to the velocity references for the vehicles, $\dot{\mathbf{x}}_{ij,ref}$, it is necessary to know the inverse of the Jacobian matrix associated to (4), so that $\dot{\mathbf{x}}_{ij,ref} = \mathbf{J}^{-1}(\mathbf{q})\dot{\mathbf{q}}_{ref}$ can be obtained. Such a relationship is obtained writing the reverse mapping correspondent to (4) and differentiating it to obtain

$$\mathbf{J}^{-1}(\mathbf{q}) = \begin{bmatrix} \mathbf{I}_{3\times3} & \mathbf{0}_{3\times3} \\ \mathbf{I}_{3\times3} & \mathbf{J}_c^{-1} \end{bmatrix}, \tag{5}$$

with

$$\mathbf{J}_c^{-1} = \begin{bmatrix} -\rho_F s_{\alpha_F} c_{\beta_F} & -\rho_F c_{\alpha_F} s_{\beta_F} & c_{\alpha_F} c_{\beta_F} \\ \rho_F c_{\alpha_F} c_{\beta_F} & -\rho_F s_{\alpha_F} s_{\beta_F} & s_{\alpha_F} c_{\beta_F} \\ 0 & \rho_F c_{\beta_F} & s_{\beta_F} \end{bmatrix}. \tag{6}$$

The stability analysis for the control law of (3) is provided, based on the theory of Lyapunov. Assuming a perfect tracking of the reference velocity by the robots, i.e., $\nu_{\mathbf{q}} = \dot{\mathbf{q}}_{ref} - \dot{\mathbf{q}} = \mathbf{0}$, the closed-loop kinematic equation can be written as

$$\dot{\mathbf{q}}_{des} + \kappa_1 \tanh(\kappa_2 \tilde{\mathbf{q}}) = \dot{\mathbf{q}}, \tag{7}$$

or

$$\dot{\tilde{\mathbf{q}}} + \kappa_1 \tanh(\kappa_2 \tilde{\mathbf{q}}) = 0. \tag{8}$$

To check the stability of the system thus described, the radial-basis function $V(\tilde{\mathbf{q}}) = \frac{1}{2}\tilde{\mathbf{q}}^\top \tilde{\mathbf{q}}$ will be used as the Lyapunov candidate function. Notice that $V(\tilde{\mathbf{q}}) > 0$ for all $\tilde{\mathbf{q}} \neq \mathbf{0}$ and $V(\tilde{\mathbf{q}}) = 0$ only for $\tilde{\mathbf{q}} = 0$, as demanded from a Lyapunov candidate function. As for the first time derivative of such a function, it is

$$\dot{V} = \tilde{\mathbf{q}}^\top \dot{\tilde{\mathbf{q}}}. \tag{9}$$

Looking for asymptotic stability, $\dot{V}$ should be negative for all $\tilde{\mathbf{q}} \neq \mathbf{0}$. In fact, introducing (8) in (9) it comes

$$\dot{V} = -\tilde{\mathbf{q}}^\top \kappa_1 \tanh(\kappa_2 \tilde{\mathbf{q}}), \tag{10}$$

allowing checking that $\dot{V} < 0$, $\forall\ \tilde{\mathbf{q}} \neq \mathbf{0}$, since $\tanh(\cdot)$ is an odd function. As a result, $\tilde{\mathbf{q}} \to \mathbf{0}$ when $t \to \infty$, allowing concluding that the proposed control law makes the system asymptotically stable.

An important detail in the development of such stability proof is that the tracking error for the reference velocities is assumed to be zero ($\nu_{\mathbf{q}} = \mathbf{0}$). This assumption can be made because the formation is a virtual structure, thus not having inertia or dynamics associated to it. In Section V-A, however, where real quadrotors are considered, the dynamic effects will be considered and such assumption will be relaxed, expanding the stability proof to consider the dynamics of the vehicles and the payload.

IV. SYSTEM DYNAMICS

The position of the i-th quadrotor in the three-dimensional space is $\mathbf{x}_i = [x_i \ y_i \ z_i]^\top$, indicating the longitudinal, lateral and normal displacements with respect to the world referential system $\langle w \rangle$. By its turn, $\eta_i = [\phi_i \ \theta_i \ \psi_i]^\top$ is a vector that contains the roll, pitch and yaw angles correspondent to the vehicle, also in $\langle w \rangle$. In other words, $\mathbf{x}_i$ and η_i represent, respectively, the translational and attitude variables associated to each UAV. The mathematical model for quadrotors is well covered in the literature, and, for the 6-DoF body in the three-dimensional space, can be given by [33]

$$m\ddot{x} = (c_\psi s_\theta + s_\psi c_\theta s_\phi)u_1 - d_1\dot{x}, \tag{11a}$$

$$m\ddot{y} = (s_\psi s_\theta - c_\psi c_\theta s_\phi)u_1 - d_2\dot{y}, \tag{11b}$$

$$m\ddot{z} = (c_\phi c_\theta)u_1 - mg - d_3\dot{z}, \tag{11c}$$

$$I_{xx}\ddot{\phi} \approx u_{2,\phi} + (I_{zz} - I_{yy})\dot{\theta}\dot{\psi} - d_4\dot{\phi}, \tag{11d}$$

$$I_{yy}\ddot{\theta} \approx u_{2,\theta} + (I_{xx} - I_{zz})\dot{\phi}\dot{\psi} - d_5\dot{\theta}, \tag{11e}$$

$$I_{zz}\ddot{\psi} \approx u_{2,\psi} + (I_{yy} - I_{xx})\dot{\phi}\dot{\theta} - d_6\dot{\psi}, \tag{11f}$$

where g is the gravity acceleration, m is the mass of the quadrotor, $\mathbf{I} = \text{diag}[I_{xx}\ I_{yy}\ I_{zz}]$ is the matrix of moments of inertia of the vehicle, $\mathbf{d} = [d_1, ..., d_6]^\top$ are the air drag coefficients, and u_1, $u_{2,\phi}$, $u_{2,\theta}$ and $u_{2,\psi}$ are the thrust and torque commands generated by the low level controllers responsible to stabilize the attitude of the vehicle.

An important remark is that to use the built-in low-level attitude controllers available in most off-the-shelf quadrotors, the payload should not affect the pitch and roll internal control loops, i.e., the payload dynamics should be decoupled from the attitude dynamics of the quadrotor. This is obtained by attaching the cable connecting the load to the quadrotor at its center-of-mass. Although being quite difficult to access the CoM in real quadrotors – it is likely to lie inside the vehicle body or components – we can adjust the attaching point at the base of the vehicle in such a way that any offset is just in the $\hat{\mathbf{z}}^w$ direction. Considering that this is done, and that the desired attitude angles are small, the payload dynamics and the quadrotor dynamics can be considered decoupled [34].

Therefore, from (11), only equations (11a)-(11c) need to be modified to include the payload dynamic effects. Considering that the payload is in equilibrium relative to the aerial vehicles, i.e., without swinging, the forces applied by the quadrotors on the load are vertical. Under such conditions internal forces are null, and each vehicle needs to adjust its thrust to carry the same additional weight, which is half of the mass of the bar ($\frac{1}{2}m_{bar}$).

Out of internal equilibrium state, the payload may swing at longitudinal and lateral planes, and twist around horizontal plane, with swing angles γ_x, γ_y, and γ_α, respectively (see Figure 1 for examples of γ_y and γ_α). Considering the payload dynamic effects as $\Delta(\cdot)$, the motion equations for a quadrotor, considering a point-mass approximation for the payload, are, then,

$$\ddot{x} = \frac{(c_\psi s_\theta + s_\psi c_\theta s_\phi)}{M}u_1 - \frac{d_1}{M}\dot{x} + \Delta(\gamma_{x,\ddot{x}}), \tag{12a}$$

$$\ddot{y} = \frac{(s_\psi s_\theta - c_\psi c_\theta s_\phi)}{M}u_1 - \frac{d_2}{M}\dot{y} + \Delta(\gamma_{y,\ddot{y}}), \tag{12b}$$

$$\ddot{z} = \frac{(c_\phi c_\theta)}{M}u_1 - g - \frac{d_3}{M}\dot{z} + \Delta(\gamma_{x,\ddot{z}}) + \Delta(\gamma_{y,\ddot{z}}), \tag{12c}$$

$$\Delta(\gamma_{x,\ddot{x}}) \approx \frac{1}{2}\left(-\frac{m_{bar}}{M}\ell c_{\gamma_x}\ddot{\gamma}_x + \frac{m_{bar}}{M}\ell s_{\gamma_x}\dot{\gamma}_x{}^2\right), \tag{12d}$$

$$\Delta(\gamma_{x,\ddot{z}}) \approx \frac{1}{2}\left(-\frac{m_{bar}}{M}\ell s_{\gamma_x}\ddot{\gamma}_x - \frac{m_{bar}}{M}\ell c_{\gamma_x}\dot{\gamma}_x{}^2\right), \tag{12e}$$

$$\ddot{\gamma}_x \approx \frac{-c_{\gamma_x}}{\ell}\ddot{x} - \frac{s_{\gamma_x}}{\ell}g, \tag{12f}$$

$$\ddot{\gamma}_y \approx \frac{-c_{\gamma_y}}{\ell}\ddot{y} - \frac{s_{\gamma_y}}{\ell}g, \tag{12g}$$

where $M \approx (m + \frac{1}{2}m_{bar})$. The effects of $\Delta\gamma_y$ are given by equations similar to (12d)-(12e), and the effects of γ_α can be interpreted as a superposition of γ_x and γ_y swinging.

V. DYNAMIC COMPENSATOR

As illustrated in Figure 3, velocity references from the kinematic formation controller, $\dot{\mathbf{x}}_{ij,ref} = \mathbf{J}^{-1}(\mathbf{q})\dot{\mathbf{q}}_{ref}$, are used to guide the aerial robots in the load transportation task, and an error in the reference tracking for each quadrotor occurs due to system dynamics. This means that

$$\nu_i = \dot{\mathbf{x}}_{i,ref} - \dot{\mathbf{x}}_i \neq 0, \quad \nu_j = \dot{\mathbf{x}}_{j,ref} - \dot{\mathbf{x}}_j \neq 0. \tag{13}$$

To reduce such velocity-tracking error an adaptive dynamic compensator is here proposed for each quadrotor, aiming at improving the performance of the whole control system. Since the same adaptive dynamic compensation module is used for both quadrotors, the i, j notations are dropped, for convenience.

Aiming at safety and accuracy, usually low or moderate velocities are used to transport payloads. Thus, a small-angle linearization can be applied to the quadrotor attitude in (12), with minor performance losses. To ensure the validity of the small-angle linearization, limits are established for the desired pitch and roll angles θ_{des} and ϕ_{des}, which are both $\leq 15°$. These limitations are equivalent to translational accelerations up to 2.5 m/s^2.

Exploiting the built-in low-level attitude controllers of the vehicles, the high-level translational inputs are the roll command u_ϕ, the pitch command u_θ, and the altitude rate command $u_{\dot{z}}$. These commands are grouped in a vector defined as $\mathbf{u} = \begin{bmatrix}u_\theta & u_\phi & u_{\dot{z}}\end{bmatrix}^\top = \begin{bmatrix}K_{u,\theta}\theta_{des} & K_{u,\phi}\phi_{des} & K_{u,\dot{z}}\dot{z}_{des}\end{bmatrix}^\top$, whose entries are all in the interval $[-1.0, +1.0]$, representing the normalized limits for the desired high-level commands, with K_u being the proportionality constants associating the normalized control commands to the embedded controller limit parameters.

Thus, (12a)-(12c) can be written as

$$\begin{aligned}
\ddot{x} &= \frac{(c_\psi\theta_{des} + s_\psi\phi_{des})}{M}u_1 - \frac{d_1}{M}\dot{x} + \Delta(\gamma_{x,\ddot{x}}),\\
\ddot{y} &= \frac{(s_\psi\theta_{des} - c_\psi\phi_{des})}{M}u_1 - \frac{d_2}{M}\dot{y} + \Delta(\gamma_{y,\ddot{y}}),\\
\ddot{z} &= \frac{1}{\tau_{\dot{z}}}(u_{\dot{z}} - \dot{z}) - \frac{d_3}{M}\dot{z} + \Delta(\gamma_{x,\ddot{x}}) + \Delta(\gamma_{y,\ddot{y}}),
\end{aligned} \tag{14}$$

where $\tau_{\dot{z}}$ is the time constant for the altitude rate.

This article has been accepted for publication in a future issue of this journal, but has not been fully edited. Content may change prior to final publication. Citation information: DOI 10.1109/ACCESS.2021.3113466, IEEE Access

Finally, the model (14) for the quadrotor can be written in the linear form as

$$\mathbf{u} = R_{\psi}^{-1}(\mathbf{A}\ddot{\mathbf{x}} + \mathbf{B}\dot{\mathbf{x}} + \Delta), \tag{15}$$

and the control law

$$\mathbf{u} = R_{\psi}^{-1}(\hat{\mathbf{A}}\ddot{\mathbf{x}}_{ref} + \hat{\mathbf{B}}\dot{\mathbf{x}} + \kappa_D \nu + \Delta) \tag{16}$$

can be adopted, where R_{ψ}^{-1} is a rotation matrix relating $\langle w \rangle$ to $\langle b \rangle$, only dependent of ψ, $\mathbf{A} = diag(a_1, a_2, a_3)$ and $\mathbf{B} = diag(b_1, b_2, b_3)$ are diagonal positive definite matrices containing the thrust-related dynamic parameters for the vehicle, ν is the tracking error between the reference velocity given by the formation kinematic controller and the velocity of the vehicle (as given in (13)), $\ddot{\mathbf{x}}_{ref}$ is the acceleration reference obtained by differentiating the reference velocity given by the formation controller ($\dot{\mathbf{x}}_{ref}$), and κ_D is a diagonal positive definite matrix. To execute the control law, the thrust-related dynamic parameters ($\hat{\mathbf{A}}$, $\hat{\mathbf{B}}$) can be estimated using a series of samples from experimental trials and least square identification, as in [35] and [36]. The yaw commands for each vehicle are not covered here, and can be selected arbitrarily, since the quadrotor is an omnidirectional vehicle.

A. ADAPTIVE DYNAMIC COMPENSATOR

From equations (14)-(16), the dynamics lumped in matrices $\mathbf{A}$ and $\mathbf{B}$ depends of u_1, g, M and the air drag coefficients. Thus, it depends on the thrust of the vehicles, and the mass and shape of the vehicles and payload. Therefore, for every different payload being carried, and for every flight mode that the system is executing, the parameters of $\mathbf{A}$ and $\mathbf{B}$ will be different (e.g., transporting a payload with different mass, or delivering the load and switching between flying with load to flying without load). Instead of using a complex hybrid model to attend the in-flight changes in the dynamics of the vehicles, we exploit the fact that the dynamics of every flight mode discussed in Section I can be obtained by changing the parameters of $\mathbf{A}$ and $\mathbf{B}$ accordingly. To change the dynamic parameters in real-time by feedback, an adaptive action is added to the proposed dynamic compensator.

Also, as shown in (12f)-(12g), the disturbances caused by the payload swinging angles, Δ, have their origin in the translational accelerations of the vehicles. Thus, to get good performance with the framework here proposed the user should choose desired trajectories with low/moderate accelerations and transportation under constant velocities. In addition, smooth accelerations are advised, with initial and final accelerations equal to zero. Following these considerations, we can assume $\Delta \approx \mathbf{0}$ during constant velocities, with minor deviations occurring when accelerating, which should be addressed by the adaptive PD feedback. These restrictions on the desired trajectories are the giveback for simplifying the proposal, allowing the control of the payload position in open-loop, thus, allowing the use of off-the-shelf quadrotors without any additional sensors. Notice that to control the payload position in open-loop, in this case, means that the closed-loop control is applied to the positions of the two quadrotors, and getting control of such positions one gets control of the load position as a consequence.

As the control law (16) depends on constant or slowly-varying terms multiplied by time-varying states, one can write the translational control law in compact form as

$$\mathbf{u} = \mathbf{G}(\ddot{\mathbf{x}}_{\mathbf{ref}}, \dot{\mathbf{x}})\hat{\Theta} + \kappa_D \nu, \tag{17}$$

with

$$\begin{bmatrix} u_\theta \\ u_\phi \\ u_{\dot{z}} \end{bmatrix} = \begin{bmatrix} \ddot{x}_{ref} & \dot{x} & 0 & 0 & 0 & 0 \\ 0 & 0 & \ddot{y}_{ref} & \dot{y} & 0 & 0 \\ 0 & 0 & 0 & 0 & \ddot{z}_{ref} & \dot{z} \end{bmatrix} \begin{bmatrix} a_1 \\ b_1 \\ a_2 \\ b_2 \\ a_3 \\ b_3 \end{bmatrix}, \tag{18}$$

and thus the parameter update rule can be selected as

$$\dot{\hat{\Theta}} = \kappa_\Theta \mathbf{G}^\top \nu, \tag{19}$$

where $\kappa_\Theta \in \mathbb{R}^{3\times3}$ is a symmetric positive definite matrix, $\mathbf{G} \in \mathbb{R}^{3\times6}$ is a regression matrix which considers the velocities and accelerations, $\Theta \in \mathbb{R}^6$ is a vector containing the constant or slowly-varying model dynamic parameters, and $\hat{\Theta}$ represents the vector of estimated dynamic parameters (characterized through $\tilde{\Theta} = \hat{\Theta} - \Theta$).

B. STABILITY ANALYSIS

In this analysis, the assumption of perfect tracking of reference velocity is relaxed, which means that the dynamics of the vehicles affect the closed-loop equations.

Taking the Lyapunov candidate function as the radial-basis function

$$V(\nu, \tilde{\Theta}) = \frac{1}{2}\nu^\top \mathbf{A}\nu + \frac{1}{2}\tilde{\Theta}^\top \kappa_\Theta^{-1}\tilde{\Theta}, \tag{20}$$

which is positive for all $\nu, \tilde{\Theta} \neq \mathbf{0}$ and null for $\nu = \mathbf{0}$ and $\tilde{\Theta} = \mathbf{0}$, the first time derivative is

$$\dot{V} = \nu^\top \mathbf{A}\dot{\nu} + \dot{\tilde{\Theta}}^\top \kappa_\Theta^{-1}\tilde{\Theta}. \tag{21}$$

Considering $\dot{\nu} = \ddot{\mathbf{x}}_{ref} - \ddot{\mathbf{x}}$, and using (15) one gets

$$\begin{aligned} \mathbf{A}\dot{\nu} &= \mathbf{A}\ddot{\mathbf{x}}_{ref} - \mathbf{A}\ddot{\mathbf{x}} \\ &= \mathbf{A}\ddot{\mathbf{x}}_{ref} + \mathbf{B}\dot{\mathbf{x}} - \mathbf{u} \\ &= \mathbf{G}\Theta - \mathbf{u} \end{aligned} \tag{22}$$

Introducing (22) in (21) and using the control law of (17), one gets, for the closed-loop system,

$$\dot{V} = \nu^\top \left(\mathbf{G}\Theta - \mathbf{G}\hat{\Theta} - \kappa_D \nu\right) + \dot{\tilde{\Theta}}^\top \kappa_\Theta^{-1}\tilde{\Theta}. \tag{23}$$

which simplifies to

$$\dot{V} = -\nu^\top \kappa_D \nu + \left(-\nu^\top \mathbf{G} + \dot{\tilde{\Theta}}^\top \kappa_\Theta^{-1}\right)\tilde{\Theta} \tag{24}$$

Now, considering $\dot{\tilde{\Theta}} = \dot{\hat{\Theta}}$, since the vector of real parameters Θ can be considered constant or slowly-varying for a given

flight mode or configuration ($\dot{\Theta} = 0$), and inserting the adaptive law (19) in (24), one finally gets

$$\begin{aligned} \dot{V} &= -\nu^\top \kappa_D \nu + \left(-\nu^\top \mathbf{G} + \nu^\top \mathbf{G}\right)\tilde{\Theta} \\ \dot{V} &= -\nu^\top \kappa_D \nu \leq 0. \end{aligned} \tag{25}$$

Using the Barbalat's lemma [37], the result in (25) implies that for bounded desired trajectories, and considering that the input for the quadrotors $\mathbf{u}$ is bounded, $\ddot{V}$ is bounded, and, therefore, $\dot{V}$ is uniformly continuous, which implies in asymptotically stable velocity tracking. In other words, $\nu \to 0$, which also implies that $\dot{\tilde{\mathbf{x}}}, \tilde{\mathbf{x}} \to 0$ asymptotically. Therefore, the proposed adaptive dynamic controller guarantees the asymptotic convergence of the real velocities to the reference velocities given by the kinematic formation controller and the positions of the vehicles to the desired positions.

VI. EXPERIMENTAL SETUP

To validate the proposed algorithms, extensive real-world experiments were run using two *Parrot Bebop 2* quadrotors to carry an aluminum bar measuring $L = 1.45$ m and weighing 155 g. Each robot weighs 500 g, and the load is attached to the robots through flexible cables.

The algorithms run in an offboard station, at a rate of 30 Hz, acquiring the poses of the vehicles and the payload through an *OptiTrack* motion capture system configured with eight cameras, and computing the reference control signals that are sent to the robots via ROS.

As stated in Section III, the formation controller is responsible for receiving the desired navigation references and evaluate the reference velocities that each robot should attain to accomplish the mission. According to Subsection V-A, uncertainties from the model and payload are handled by the adaptive dynamic compensation module, as well as the ability to fly in different flight modes. The initial dynamic parameters for $\hat{\mathbf{A}}$ and $\hat{\mathbf{B}}$ were obtained according to the method presented in Section V, considering a single quadrotor flying without a payload, and are given by $\mathbf{A} = diag(0.39,\ 0.4,\ 0.25)$ and $\mathbf{B} = diag(0.21,\ 0.20,\ 1.01)$. It is worthy mentioning, however, that due to the adaptive action of the dynamic compensator, such an identification process can be completely skipped. Indeed, the dynamic parameter matrices $\hat{\mathbf{A}}$ and $\hat{\mathbf{B}}$ could be both initialized as the unit matrix $\mathbf{I}_{3\times 3}$. Then, low acceleration trajectories should be performed for a few seconds, thus allowing the algorithm to stabilize and online adapt the parameters to the optimal values.

With regard to the validating experiments, five transportation tasks were executed to test the proposed algorithms. In every experiment, the control of the payload position, $\mathbf{x}_{bar}$, and orientation, η_{bar}, is the main concern. Hence, following the control structure presented in Figure 3, the desired payload state is the task planner input, from which $\mathbf{q}_{p,des}$ and $\dot{\mathbf{q}}_{p,des}$ are obtained using (2), and $\mathbf{q}_{c,des} = [\psi_{bar,des} \quad \theta_{bar,des} \quad L]^\top$. The payload roll angle, ϕ_{bar}, is not possible to be controlled using our proposal. Also, the yaw angle for the vehicles are not considered, because the quadrotor is an omnidirectional vehicle, as mentioned in Section IV.

As for the gains adopted for the controller of each quadrotor in the experiments discussed ahead, they are the diagonal matrices $\kappa_1 = diag(2.5, 2.5, 3.0, 2.0, 2.0, 2.0)$, $\kappa_2 = diag(1.0, 1.0, 1.0, 1.0, 1.0, 1.0)$, $\kappa_D = diag(2.7, 2.7, 3.0)$, and $\kappa_\Theta = 10^{-3} diag(1.0, 0.1, 1.0, 0.1, 2.0, 5.0)$.

VII. RESULTS

In this section, the results that validate the proposals here reported are presented. Considering that a successful transportation is one that is precise and safe, the aimed performance in the following trials, so-called a good tracking performance, are position errors around 15 cm (or error norm around $||\mathbf{x}_{bar}||_2 = 15\sqrt{3} \approx 26$ cm) and orientation errors around 10°. All error metrics presented in the following were measured considering the center of mass of the transported bar. As our objective is to propose a robust and simple controller for load transportation, simplicity and robustness were preferred, over higher precision.

To test the robustness of our system, we impose the following challenges in the transportation experiments: high payload-to-quadrotor weight ratio, 20% of error in the model parameters of the vehicles, transport under wind-like disturbances, manipulation of the payload orientation during transport, and changes of the payload weight during transportation. We also tested our system using moderate velocities and accelerations, aiming at practical applications, where a robust but not sluggish system is preferred. A video showcasing our system under these challenges can be watched at https://youtu.be/eDFRapPJQ18.

In the following subsections, we further analyze the results obtained in each experiment. Although this proposal does not demand payload information to feedback the controllers, in the experiments run the *OptiTrack* system was also used to measure the position of the center of mass of the payload, just to produce the graphics shown.

A. TASK #1: TRANSPORTATION AT HIGH ACCELERATIONS AND PAYLOAD WEIGHT - COMPARISON WITH PID

In task #1 the bar is transported through a tilted lemniscate-shape trajectory parameterized as

$$\mathbf{x}_{bar,des} = \begin{bmatrix} r_x \cos\dfrac{2\pi t}{T} & r_y \sin\dfrac{4\pi t}{T} & z_0 + r_z \sin\dfrac{4\pi t}{T} \end{bmatrix}^\top, \tag{26}$$

where $r_x = r_y = 1$ m, $r_z = 0.35$ m, $z_0 = 0.55$ m, and $T = 16$ s. The length of the cable attached to the payload is $\ell = 0.8$ m. Further, we attached an additional payload, weighing 180 g, nearby the CoM of the bar. Therefore, for this experiment, the total payload mass is 335 g and the payload-to-quadrotors weight ratio is 0.335, once our vehicles weights 1000 g combined. To avoid excessive oscillations, acceleration and deceleration phases were used, to smoothly increase and decrease the trajectory frequency, whose duration was 10 s and 5 s, respectively.

This article has been accepted for publication in a future issue of this journal, but has not been fully edited. Content may change prior to final publication. Citation information: DOI 10.1109/ACCESS.2021.3113466, IEEE Access

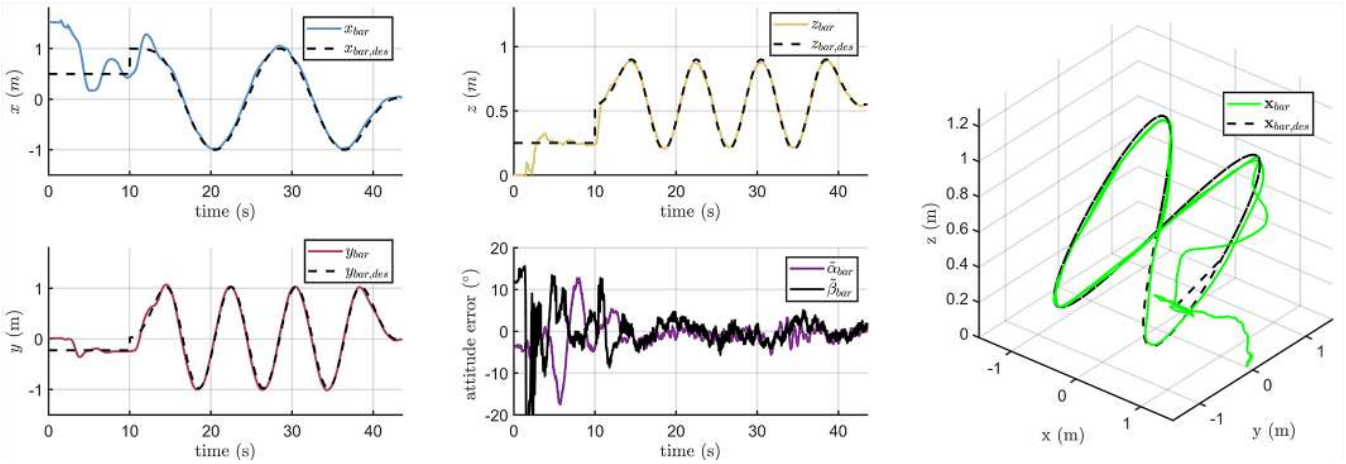

FIGURE 4. The tracking error for the payload center-of-mass using the proposed adaptive controller during transportation task #1.

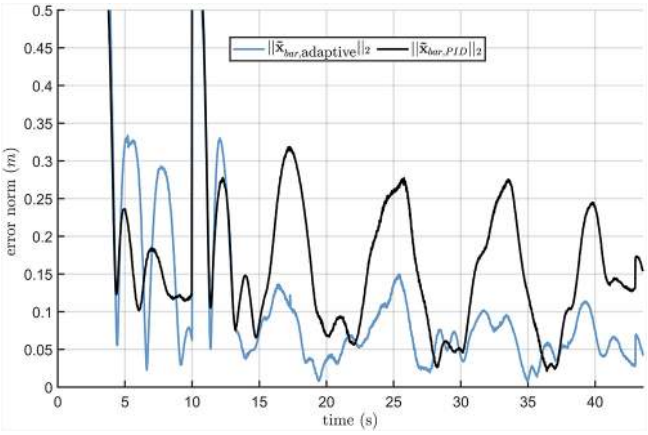

FIGURE 5. Norm of the error for the adaptive and PID controllers during transportation task #1.

To compare our approach to commonly used robust methods, we benchmark our controller with a well-tuned PID controller. The performance of our approach is presented in Figure 4. For the PID controller, several runs were performed with different parameters, and the PID gains which generated the best performance were adopted. For the sake of comparison, the norm of the error is presented in Figure 5, considering the controller here proposed and the PID one. As one can see from such a figure, our adaptive controller overperforms the PID controller after having its parameters adapted.

In another test, we further increased the desired acceleration in (26) by decreasing the period to $T = 10$ s, which is equivalent to maximum desired acceleration of 1.6 m/s^2. In Figure 6 it is possible to see the performance obtained using our approach. We also tried to use a PID controller in this case, for comparison, but the PID controller was not able to accomplish the task, leading to crashes or tracking errors above 50 cm.

B. TASK #2: TRANSPORTATION WITH PARAMETER UNCERTAINTIES

In this task, the desired trajectory in (26) was used once again, but here we purposely introduced an error in the identified values of the dynamic parameters, presented in Section VI, of around 20%. This test was motivated by a commonly found scenario in real-world applications, where the identified parameters are far from the real ones due to adverse conditions of the vehicle (e.g., component wearing) and environment. In this kind of scenario, adaptive systems are superior due to their parameter adjustment nature, in opposition to PID systems, which are very restricted when regarding the kind of uncertainty that the system undergoes.

The performance comparison between the proposed adaptive controller and the PID controller can be seen in Figure 7, where just the norm of the error is presented, due to the similarity of the component-wise performance to already presented graphs (as the one in Figure 4). As expected, the adaptation of the thrust-related dynamic parameters is able to greatly improve the tracking performance under parameter uncertainties in comparison to integral offset correction. In short, the robustness obtained by PID controllers is restricted, at best, to slowly-varying time-varying states or disturbances, not being well-suited to address the errors caused by misidentification of $\hat{\mathbf{A}}$ or $\hat{\mathbf{B}}$.

C. TASK #3: TRANSPORTATION UNDER WIND-LIKE DISTURBANCES

To validate our algorithms for transportation under windy environments, we emulate the dynamical forces caused by opposing wind in quadrotors, attaching to the top of the vehicles a foam plate of 25x25 cm^2, as shown in Figure 8. These foam plates generate opposing drag forces when the quadrotors try to track the trajectories and when they accelerate to compensate for the disturbances. To demonstrate the effects caused solely by those plates, we guided one of the quadrotors through a lemniscate trajectory in two runs, one with and one without the foam plate, and the results of this

This article has been accepted for publication in a future issue of this journal, but has not been fully edited. Content may change prior to final publication. Citation information: DOI 10.1109/ACCESS.2021.3113466, IEEE Access

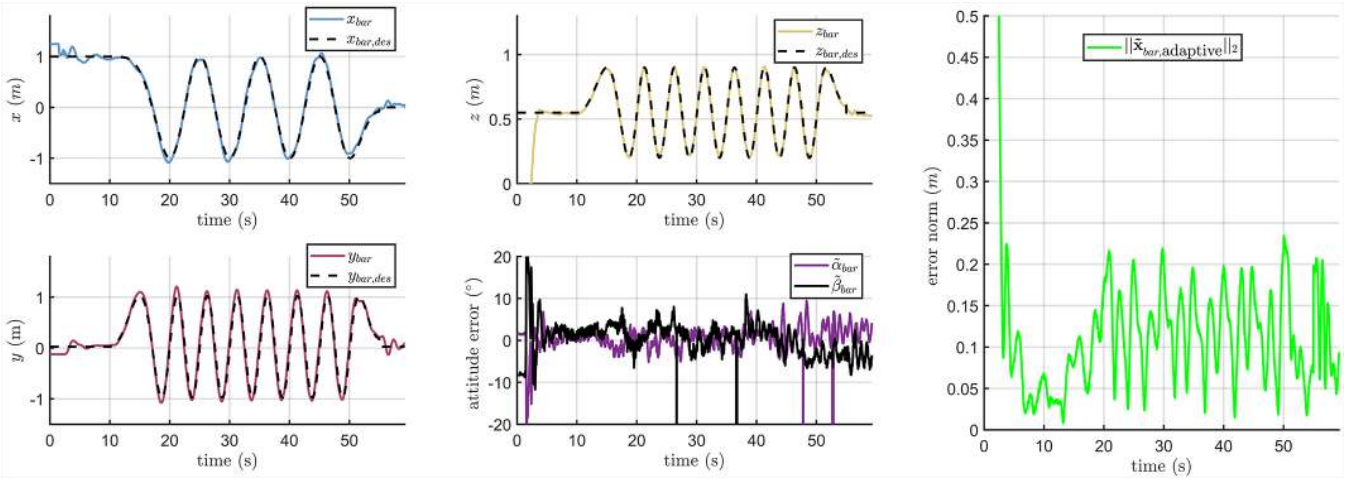

FIGURE 6. The tracking error for the payload center-of-mass using the adaptive controller under accelerations up to 1.6 m/s^2 for task #1.

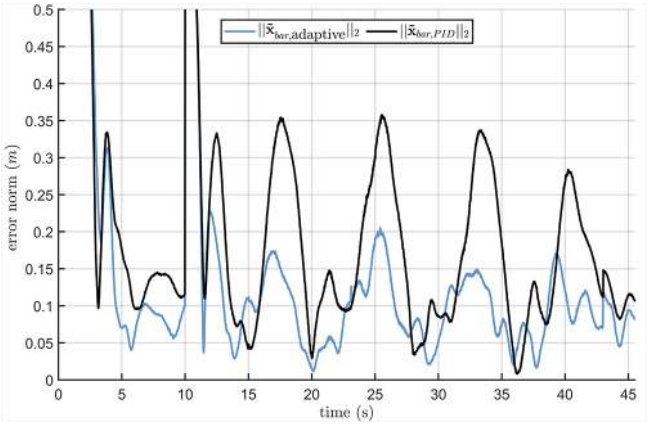

FIGURE 7. Norm of the payload CoM error for the adaptive and PID controllers during transportation task #2.

FIGURE 8. Experimental setup containing the used quadrotors, bar-shaped payload, and drag foam plates.

experiment are shown in Figure 9.

As one can perceive in Figure 9, the foam plate directly impacts in the tracking performance, but, as our approach adapts for drag in the parameter $\hat{\mathbf{B}}$ in (16), we expect that the opposing drag forces are counteracted by the proposed controller. To verify it, we maneuver the payload in a co-operative transportation through a circular-shaped trajectory parameterized as

$$\mathbf{x}_{bar,des} = \begin{bmatrix} r_x \sin\dfrac{2\pi t}{T} & r_y \cos\dfrac{2\pi t}{T} & z_0 \end{bmatrix}^\top, \qquad (27)$$

where $r_x = r_y = 1$ m, $z_0 = 0.55$ m, and $T = 5$ s, which corresponds to translational accelerations up to 1.6 m/s^2. The combined load of the two foam plates and the bar-shaped payload during this transportation was 275 g, corresponding to a weight ratio of 0.275. The trajectory tracking results for such experiment are shown in Figure 10. As one can see, the impact of opposed drag forces is counteracted by adapting the dynamic parameters involved in the controller. We also tried to compare the results obtained using our approach to

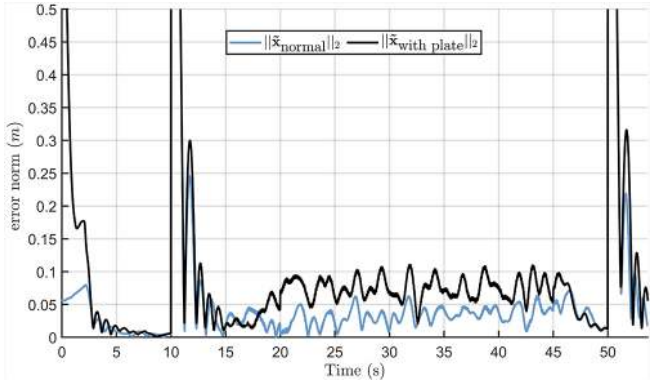

FIGURE 9. The norm of the translational error for a quadrotor without the foam plate (blue), and with the foam plate (black). Test used for transportation task #3.

This article has been accepted for publication in a future issue of this journal, but has not been fully edited. Content may change prior to final publication. Citation information: DOI 10.1109/ACCESS.2021.3113466, IEEE Access

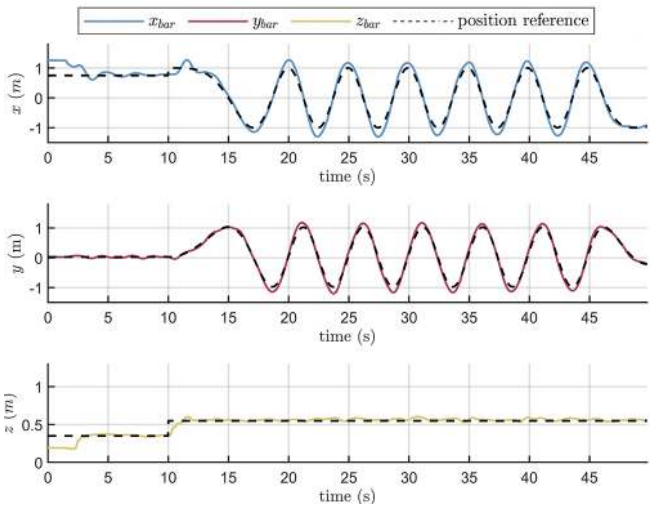

FIGURE 10. Trajectory tracking for the payload center-of-mass considering additional drag forces under accelerations up to 1.6 m/s^2 during transportation task #3.

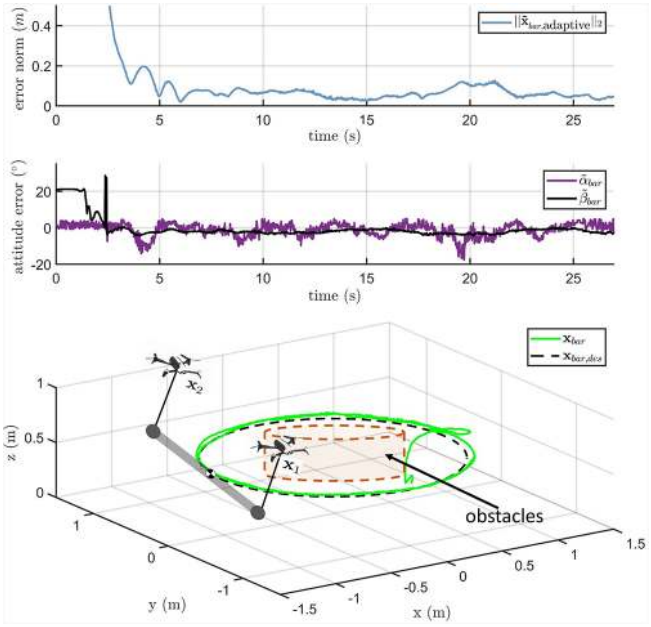

FIGURE 11. The tracking error norm, attitude error, and 3D view for task #4.

standard PID controller, but it resulted in crashes in all of our tries. The conclusion is that PID-based systems are not able to deal with this kind of disturbance.

D. TASK #4: MANEUVERING THE PAYLOAD TO AVOID OBSTACLES

The approach here proposed allows the manipulation of the payload translational positions and attitude angles, except for roll angle. Therefore, it is possible to propose desired trajectories and paths including maneuvers allowing the payload to avoid obstacles.

In this fourth task, the payload should contour obstacles in the center of the testing area, emulating the necessary manipulation used in narrow corridors, for instance, where the payload should be turned to go on in corners. This maneuver is represented by a circular-shaped trajectory parameterized as in (27), with $r_x = r_y = 1$ m, $z_0 = 0.55$ m, and $T = 9$ s. The cable lengths are $\ell = 0.8$ m.

To contour the circular trajectory, the payload desired orientation is given by the tangent of the trajectory, such that $\alpha_{bar,des} = \text{atan2}\,(y_{bar}, x_{bar}) - 180°$, where $-180°$ was used for quadrotor $\mathbf{x}_1$ to lead the formation. We also tilted the payload with $\beta_{bar,des} = 20°$, emulating a tilt that might be necessary to transport the payload in stairs or inclined surfaces, such as access ramps.

The obtained performance is presented in Figure 11. It is possible to see that the desired performance was achieved in the accomplishment of this task.

E. TASK #5: UNBALANCED LOAD TRANSPORTATION

This last transportation task consists of carrying the bar through a tilted lemniscate-shape trajectory parameterized as

$$\mathbf{x}_{bar,des} = \begin{bmatrix} r_x \sin\dfrac{4\pi t}{T} & r_y \cos\dfrac{2\pi t}{T} & z_0 + r_z \sin\dfrac{4\pi t}{T} \end{bmatrix}^\top, \quad (28)$$

where $r_x = r_y = 1$ m, $r_z = 0.35$ m, $z_0 = 0.45$ m, and $T = 30$ s. The cable lengths are $\ell = 1.15$ m. Once again we chose a trajectory that excites the system dynamics in three dimensions, with smooth sinusoidal acceleration. Also, during the transportation the payload should be oriented so that $\psi_{bar,des} = 90°$ and $\theta_{bar,des} = 0°$.

During the transportation, additional loads were attached to the extremities of the bar, to unbalance it. After one lemniscate cycle, in $t = 30$ s, a load weighing 180 g was added to one extremity of the bar, and after an additional cycle, in $t = 60$ s, a load weighing 240 g was added to the other extremity. The intent of this experiment is to verify if the proposed control system is able to deal with load fluctuations or loads that do not have uniform mass distribution. The final payload-to-quadrotors weight ratio was 0.575.

Figure 12 shows the graphics correspondent to the payload desired and current positions, and Figure 13 shows the graphics correspondent to the position and orientation tracking errors. In both figures, enumerated timestamps indicate the instants during the experiment in which a transition occurs (e.g., an additional payload is added to the bar, the system goes to a halt).

Analyzing such figures, one can see that the control system here proposed is able to handle the disturbances corresponding to the load oscillations and the load fluctuations due to the uneven addition of extra loads at the extremities of the bar being transported. As exhibited in Figure 13, the position tracking errors are around the expected performance after stabilization. The timestamps ① and ② indicate the time instants where the 180 g and 240 g additional payloads were inserted, respectively. It is important to notice the quick response of the proposed system during these instants, where

This article has been accepted for publication in a future issue of this journal, but has not been fully edited. Content may change prior to final publication. Citation information: DOI 10.1109/ACCESS.2021.3113466, IEEE Access

an increase in the tracking error can be easily noticed in Figure 13, which is quickly damped by the control action. Moreover, these instants are critical not only due to the need for online adaptation of the thrust of the vehicles, but also due to the external disturbances caused by the operator manipulation of the aluminum bar payload to attach the additional weight. These external perturbations cause oscillations and swings of the payload, as well as moments in which the payload exerts less force on the vehicles because the bar is held by the operator.

A 3D view of the path followed by the vehicles and the load is shown in Figure 14, in which one can check the performance of the whole system in the task accomplishment.

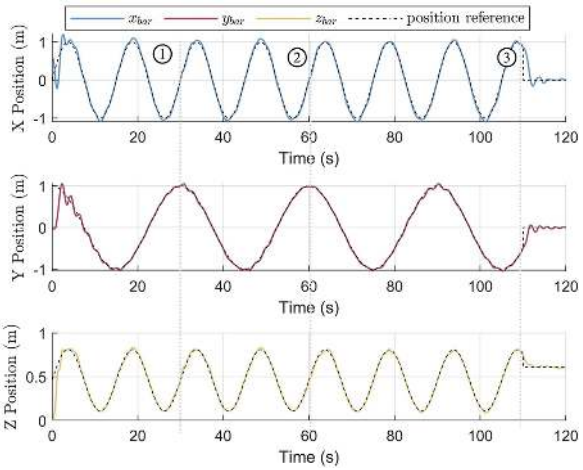

FIGURE 12. The current and desired positions for the payload center-of-mass during transportation task #5.

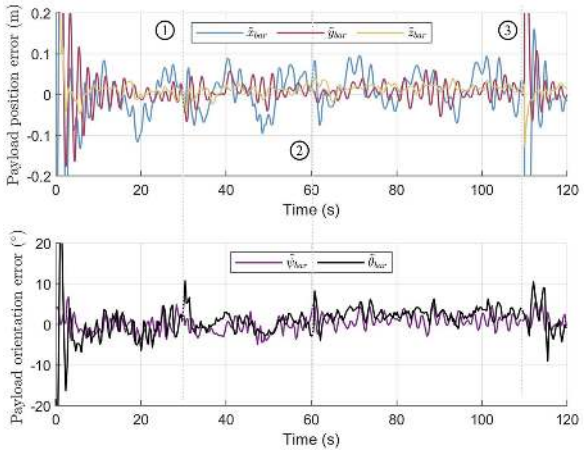

FIGURE 13. Tracking error for the position of the payload center-of-mass and for the payload orientation during transportation task #5.

Another important time interval to be checked in this experiment is the acceleration phase from rest to the timestamp ①, where we decided not to use a smooth increase in the desired trajectory frequency, which induce oscillations due to three initial conditions: (*i*) as pointed in Figure 14, the payload starting point is not on the trajectory to be tracked,

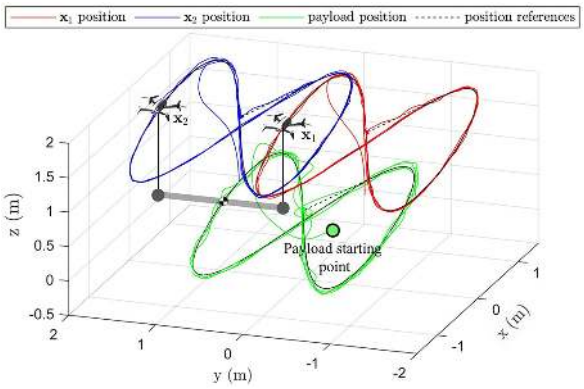

FIGURE 14. Three dimensional tracking performance for the whole system, payload and quadrotors, during transportation task #5.

making initial $\tilde{\mathbf{q}}$ big; (*ii*) as one can see in the video, the payload lifting and transportation modes occur simultaneously; and (*iii*) the desired acceleration in the $\hat{\mathbf{y}}^w$ direction depends on $cos(t)$, thus starting at its maximum value. Despite these adverse initial conditions, one can check that the oscillations are quickly damped and the transportation becomes smooth in just a few seconds.

Finally, in the timestamp ③, the trajectory tracking is halted by the operator, and a positioning task is commanded, with desired state for the payload $\mathbf{x}_{bar,des} = [0 \quad 0 \quad 0.6]^\top$ m. As discussed through this manuscript, this discontinuity induces oscillations on the payload and should be avoided. However, here it is was introduced with the purpose of performance analysis. As shown in Figure 12, the proposed algorithms can counteract the disturbances and accomplish the positioning task. As a result, the same system here proposed to track a trajectory can be used to perform positioning tasks, which only demands to define constant values of the variables corresponding to the desired formation position and shape.

Despite the recommendations on Subsection V-A of using smooth desired trajectories with initial and final accelerations equal to zero and transportation under constant velocities, the experiments presented in Subsection VII-E did not follow any of these restrictions, showing the good performance of the proposed approach even when these ideal situations are not completely fulfilled.

F. RESULTS OVERVIEW

To highlight the results of our proposal in contrast with the related works presented in Section I-A, we build a comparative board that compiles the most important features, in our opinion, for load transportation with quadrotors. Further, due to the dynamic complexity of transporting payloads using quadrotors, it is difficult to provide a reliable simulation for this task, which leads us to only compare works whose algorithms were tested in experimental trials. The comparative board thus generated is shown in Table 1.

As one can see in Table 1, the results presented in this paper bring advantages and drawbacks compared to the most

This article has been accepted for publication in a future issue of this journal, but has not been fully edited. Content may change prior to final publication. Citation information: DOI 10.1109/ACCESS.2021.3113466, IEEE Access

	This paper	[11]	[17]	[22]	[24]	[27]	[29]	[30]	[31]
Control technique	Adaptive	$\mathscr{H}_\infty$	Optimal	RL	Adaptive	PB	EB	ESO	SMC
Single or cooperative transportation	Coop.	Coop.	Coop.	Single	Single	Coop.	Single	Coop.	Single
Experiments with 3D trajectories	Yes	No	No	No	No	No	No	No	Yes
Maximum acceleration (m/s^2)	1.6	QS	QS	QS	QS	QS	QS	QS	QS
Payload to quadrotor-weight ratio	0.33 to 0.57	0.11	0.16	0.18	0.20	0.20	0.06	0.09	0.11
Payload tracking precision	Low	High	High	High	High	Low	High	Low	High
Payload orientation	2 DoF	3 DoF	3 DoF	No	No	No	No	No	no
Tested against uncertainties	Yes	Yes	Yes	Yes	Yes	Yes	Yes	Yes	Yes
Tested against wind	Yes	No	Yes	No	No	Yes	No	Yes	Yes
Tested in outdoors	No	No	Yes	No	No	No	No	Yes	No
Robust against disturbances	No	No	No	No	Yes	Yes	No	Yes	Yes
Implementation complexity	Low	Med.	High	High	Med.	Low	Low	Med.	Low

TABLE 1. Comparison among recent publications on load transportation. QS – Quasi-Static; RL – Reinforcement Learning; PB – Passivity-Based; EB – Energy-based; ESO – Extended State Observer; SMC – Sliding Mode Control; DoF – Degree of Freedom;

recent works on the subject of load transportation using quadrotors. As main advantages, our proposal manipulate and transport the payload in velocities and accelerations far from quasi-static motion, which is important considering real-world applications. In addition, we also consider heavier payloads than the rest of the compared works. Another advantage is the simplicity of implementation and the ability to suppress drag-related uncertainties (like wind). As a drawback, since we do not use measurements from the payload, our proposal lacks precision in comparison with some of the other works. In our approach, the payload is attached to the vehicles by the flexible cables, so that it is only restricted to be near of the vehicles during transportation. Aiming at getting an approach that is safe and readily applicable to off-the-shelf quadrotors, we gave more emphasis to simplicity over precision. Another important drawback is the lack of outdoor tests, which is our main objective for future works.

VIII. CONCLUDING REMARKS

The control system here proposed deals with a formation of two quadrotors transporting a rod-shaped load. Adverse conditions for the transporting were tested in real experiments, and the system presented good performance in all of them. In most of these tests, we compared our control paradigm with the PID controller, a industrial standard, and the results demonstrated the superiority of our approach. As a result, we claim that the proposed control system is able to guide the formation in the accomplishment of trajectory tracking tasks, positioning, and load-orientation tasks when transporting a rod-shaped payload.

As future works, we plan to completely get rid of the motion capture system, moving one step further towards a system applicable to real-world scenarios. Solutions for an increased number of vehicles are also being pursued, aiming at the possibility of transporting heavier payloads.

ACKNOWLEDGMENT

The authors thank CNPq – Conselho Nacional de Desenvolvimento Científico e Tecnológico, an agency of the Brazilian Ministry of Science, Technology, Innovations and Communications that supports scientific and technological development, as well as FAPES – Fundação de Amparo à Pesquisa e Inovação do Espírito Santo, an agency of the State of Espírito Santo, Brazil, that supports scientific and technological development – for financing this project. Mr. Daniel Villa also thanks Fundação CAPES – Coordenação de Aperfeiçoamento de Pessoal de Nível Superior, an agency of the Brazilian Ministry of Education that supports human resources perfectioning, for the scholarship that allowed him to develop his Ph.D. studies, in where this work is inserted. Dr. Brandão also thanks FAPEMIG – Fundação de Amparo à Pesquisa de Minas Gerais – for supporting his participation in this work. They all thank João Vasconcelos, Vinicius Pacheco Bacheti and Alexandre Caldeira, for their helpful assistance in setting up the ROS system and during the experiments run. Finally, they are also grateful to the Federal University of Espirito Santo (LAI - Laboratory of Intelligent Automation) and Federal University of Viçosa (NERO - Robotics Specialization Center).

REFERENCES

[1] A. Ollero, M. Tognon, A. Suarez, D. Lee, and A. Franchi, "Past, present, and future of aerial robotic manipulators," *IEEE Transactions on Robotics*, vol. Early Access, pp. 1–20, 2021.

[2] S. Tang and V. Kumar, "Autonomous flight," *Annual Review of Control, Robotics, and Autonomous Systems*, vol. 1, pp. 29–52, 2018.

[3] A. Mohiuddin, T. Tarek, Y. Zweiri, and D. Gan, "A survey of single and multi-uav aerial manipulation," *Unmanned Systems*, vol. 8, no. 02, pp. 119–147, 2020.

[4] D. K. Villa, A. S. Brandao, and M. Sarcinelli-Filho, "A survey on load transportation using multirotor uavs," *Journal of Intelligent & Robotic Systems*, vol. 98, no. 2, pp. 267–296, 2020.

[5] M. E. Guerrero-Sánchez, R. Lozano, P. Castillo, O. Hernández-González, C. García-Beltrán, and G. Valencia-Palomo, "Nonlinear control strategies for a uav carrying a load with swing attenuation," *Applied Mathematical Modelling*, vol. 91, pp. 709–722, 2021.

[6] P. Foehn, D. Falanga, N. Kuppuswamy, R. Tedrake, and D. Scaramuzza, "Fast trajectory optimization for agile quadrotor maneuvers with a cable-suspended payload," in *Robotics: Science and Systems*, 2017, pp. 1–10.

[7] G. Loianno, V. Spurny, J. Thomas, T. Baca, D. Thakur, D. Hert, R. Penicka, T. Krajnik, A. Zhou, A. Cho *et al.*, "Localization, grasping, and transportation of magnetic objects by a team of mavs in challenging desert-like environments," *IEEE Robotics and Automation Letters*, vol. 3, no. 3, pp. 1576–1583, 2018.

[8] S. Tang, K. Sreenath, and V. Kumar, "Multi-robot trajectory generation for an aerial payload transport system," in *Robotics Research*. Springer, 2020, pp. 1055–1071.

[9] K. Klausen, C. Meissen, T. I. Fossen, M. Arcak, and T. A. Johansen, "Cooperative control for multirotors transporting an unknown suspended load under environmental disturbances," *IEEE Transactions on Control Systems Technology*, vol. 28, no. 2, pp. 653–660, 2018.

[10] J. Horyna, T. Baca, and M. Saska, "Autonomous collaborative transport of a beam-type payload by a pair of multi-rotor helicopters," in *2021 International Conference on Unmanned Aircraft Systems (ICUAS)*. IEEE, 2021, pp. 1139–1147.

[11] D. Sanalitro, H. J. Savino, M. Tognon, J. Cortés, and A. Franchi, "Full-pose manipulation control of a cable-suspended load with multiple uavs under uncertainties," *IEEE Robotics and Automation Letters*, vol. 5, no. 2, pp. 2185–2191, 2020.

[12] J. Erskine, A. Chriette, and S. Caro, "Wrench analysis of cable-suspended parallel robots actuated by quadrotor unmanned aerial vehicles," *Journal of Mechanisms and Robotics*, vol. 11, no. 2, p. 020909, 2019.

[13] Z. Li, J. Erskine, S. Caro, and A. Chriette, "Design and control of a variable aerial cable towed system," *IEEE Robotics and Automation Letters*, vol. 5, no. 2, pp. 636–643, 2020.

[14] A. Tagliabue, M. Kamel, R. Siegwart, and J. Nieto, "Robust collaborative object transportation using multiple mavs," *The International Journal of Robotics Research*, vol. 38, no. 9, pp. 1020–1044, 2019.

[15] C. Gabellieri, M. Tognon, D. Sanalitro, L. Pallottino, and A. Franchi, "A study on force-based collaboration in swarms," *Swarm Intelligence*, vol. 14, no. 1, pp. 57–82, 2020.

[16] J. Geng, P. Singla, and J. W. Langelaan, "Trajectory planning and control for a multilift system based on load distribution," in *AIAA Scitech 2021 Forum*, 2021, p. 0980.

[17] J. Geng and J. W. Langelaan, "Cooperative transport of a slung load using load-leading control," *Journal of Guidance, Control, and Dynamics*, vol. 43, no. 7, pp. 1313–1331, 2020.

[18] T. Chen, J. Shan, and H. H. Liu, "Cooperative transportation of a flexible payload using two quadrotors," *Journal of Guidance, Control, and Dynamics*, pp. 1–9, 2021.

[19] K. Gkountas and A. Tzes, "Leader/follower force control of aerial manipulators," *IEEE Access*, vol. 9, pp. 17 584–17 595, 2021.

[20] E. Rossi, M. Tognon, R. Carli, L. Schenato, J. Cortés, and A. Franchi, "Cooperative aerial load transportation via sampled communication," *IEEE Control Systems Letters*, vol. 4, no. 2, pp. 277–282, 2019.

[21] S. Thapa, H. Bai, and J. Á. Acosta, "Cooperative aerial manipulation with decentralized adaptive force-consensus control," *Journal of Intelligent & Robotic Systems*, vol. 97, no. 1, pp. 171–183, 2020.

[22] S. Belkhale, R. Li, G. Kahn, R. McAllister, R. Calandra, and S. Levine, "Model-based meta-reinforcement learning for flight with suspended payloads," *IEEE Robotics and Automation Letters*, vol. 6, no. 2, pp. 1471–1478, 2021.

[23] X. Li, J. Zhang, and J. Han, "Trajectory planning of load transportation with multi-quadrotors based on reinforcement learning algorithm," *Aerospace Science and Technology*, p. 106887, 2021.

[24] V. P. Tran, F. Santoso, M. Garratt, and S. Anavatti, "Neural network-based self-learning of an adaptive strictly negative imaginary tracking controller for a quadrotor transporting a cable-suspended payload with minimum swing," *IEEE Transactions on Industrial Electronics*, 2020.

[25] V. P. Tran, F. Santoso, and M. A. Garratt, "Adaptive trajectory tracking for quadrotor systems in unknown wind environments using particle swarm optimization-based strictly negative imaginary controllers," *IEEE Transactions on Aerospace and Electronic Systems*, 2021.

[26] F. Rossomando, C. Rosales, J. Gimenez, L. Salinas, C. Soria, M. Sarcinelli-Filho, and R. Carelli, "Aerial load transportation with multiple quadrotors based on a kinematic controller and a neural smc dynamic compensation," *Journal of Intelligent & Robotic Systems*, vol. 100, no. 2, pp. 519–530, 2020.

[27] K. Mohammadi, S. Sirouspour, and A. Grivani, "Passivity-based control of multiple quad-rotors carrying a cable-suspended payload," *IEEE/ASME Transactions on Mechatronics*, 2021.

[28] ——, "Control of multiple quad-copters with a cable-suspended payload subject to disturbances," *IEEE/ASME Transactions on Mechatronics*, vol. 25, no. 4, pp. 1709–1718, 2020.

[29] S. Yang and B. Xian, "Energy-based nonlinear adaptive control design for the quadrotor uav system with a suspended payload," *IEEE Transactions on Industrial Electronics*, vol. 67, no. 3, pp. 2054–2064, 2019.

[30] Y. Liu, F. Zhang, P. Huang, and X. Zhang, "Analysis, planning and control for cooperative transportation of tethered multi-rotor uavs," *Aerospace Science and Technology*, vol. 113, p. 106673, 2021.

[31] R. Falcón, H. Ríos, and A. Dzul, "Comparative analysis of continuous sliding-modes control strategies for quad-rotor robust tracking," *Control Engineering Practice*, vol. 90, pp. 241–256, 2019.

[32] M. A. Lewis and K.-H. Tan, "High precision formation control of mobile robots using virtual structures," *Autonomous Robots*, vol. 4, no. 4, pp. 387–403, October 1997.

[33] L. V. Santana, A. S. Brandão, and M. Sarcinelli-Filho, "Navigation and cooperative control using the ar.drone quadrotor," *Journal of Intelligent & Robotic Systems*, vol. 84, no. 1, pp. 327–350, December 2016.

[34] J. Zeng and K. Sreenath, "Geometric control of a quadrotor with a load suspended from an offset," in *2019 American Control Conference (ACC)*. IEEE, 2019, pp. 3044–3050.

[35] M. C. P. Santos, C. D. Rosales, M. Sarcinelli-Filho, and R. Carelli, "A novel null-space-based uav trajectory tracking controller with collision avoidance," *IEEE/ASME Transactions on Mechatronics*, vol. 22, no. 6, pp. 2543–2553, December 2017.

[36] A. O. Pinto, H. N. Marciano, V. P. Bacheti, M. S. M. Moreira, A. S. Brandão, and M. Sarcinelli-Filho, "High-level modeling and control of the *Bebop 2* micro aerial vehicle," in *To appear in the Proceedings of the 2020 International Conference on Unmanned Aircraft Systems*. Athens, Greece: IEEE, September 2020, pp. 939–947.

[37] J.-J. Slotine and W. Li, *Applied Nonlinear Control*. Prentice-Hall, Inc, 1991.

DANIEL KHEDE DOURADO VILLA received the B.S. degree in Electrical Engineering and the M. Sc. degree in Agricultural Engineering, both from Federal University of Viçosa, Brazil, in 2014 and 2017, respectively. He is currently pursuing a Ph.D. degree in Electrical Engineering at the Federal University of Espírito Santo. His research interest is control of multi-robot systems applied to load transportation with aerial robots.

ALEXANDRE SANTOS BRANDÃO received the B.S. degree in Electrical Engineering from Federal University of Viçosa, Minas Gerais, Brazil, in 2006, and the M. Sc. and Ph. D. degrees, also in Electrical Engineering, from Federal University of Espírito Santo, Brazil, in 2008 and 2013, respectively. He also received the Ph.D. degree in Control System Engineering from the National University of San Juan, San Juan, Argentine, in 2014. He is currently adjunct professor of the Department of Electrical Engineering of the Federal University of Viçosa, Brazil. He has co-authored more than 20 journal papers and more than 120 conference papers. His research interests are nonlinear control of aerial and terrestrial mobile vehicles and control of multi-robot systems.

RICARDO CARELLI (M'76 - SM'98) was born in San Juan, Argentina. He graduated in Engineering from the National University of San Juan, Argentina, and obtained a Ph.D degree in Electrical Engineering from the National University of Mexico (UNAM). He is full professor at the National University of San Juan and senior researcher of the National Council for Scientific and Technical Research (CONICET, Argentina). He has co-authored more than 110 journal papers, more than 220 conference papers, besides 18 book chapters. His research interests are on Robotics, Manufacturing Systems, Adaptive Control and Artificial Intelligence Applied to Automatic Control. Prof. Carelli is a senior member of IEEE and a member of AADECA-IFAC.

MÁRIO SARCINELLI-FILHO received the B.S. degree in Electrical Engineering from Federal University of Espírito Santo, Brazil, in 1979, and the M. Sc. and Ph. D. degrees, also in Electrical Engineering, from Federal University of Rio de Janeiro, Brazil, in 1983 and 1990, respectively. He is currently a Professor at the Department of Electrical Engineering, Federal University of Espírito Santo, Brazil, a researcher of the Brazilian National Council for Scientific and Technological Development (CNPq), and Senior Editor of the Journal of Intelligent and Robotic Systems. He has co-authored more than 60 journal papers, more than 340 conference papers, and 17 book chapters. He has also advised 20 Ph.D. students and 25 M.Sc. students. His research interests are nonlinear control, mobile robot navigation, coordinated control of mobile robots, unmanned aerial vehicles and coordinated control of ground and aerial robots.